Journal of Power Sources 219 (2012) 52–59

Contents lists available at SciVerse ScienceDirect

Journal of Power Sources

journal homepage: www.elsevier.com/locate/jpowsour

Effect of clamping pressure on ohmic resistance and compression of gas diffusion layers for polymer electrolyte fuel cells

Thomas J. Mason [a], Jason Millichamp [a], Tobias P. Neville [a], Ahmad El-kharouf [b], Bruno G. Pollet [c], Daniel J.L. Brett [a,*]

[a] Centre for CO_2 Technology, Department of Chemical Engineering, UCL, Torrington Place, London WC1E 7JE, UK
[b] Centre for Hydrogen and Fuel Cell Research, School of Chemical Engineering, The University of Birmingham, Edgbaston, Birmingham B15 2TT, UK
[c] HySA Systems Competence Centre, University of the Western Cape, Private Bag X17, Bellville 7535, South Africa

HIGHLIGHTS

- Novel *in situ* method of analysis the dimensional change of PEFCs.
- Compression of gas diffusion layers with electrical resistance measurements.
- Provides criteria for selection of commercially available GDL materials.
- Relationship between force, displacement and resistance is characterised.

ARTICLE INFO

Article history:
Received 17 March 2012
Received in revised form
6 July 2012
Accepted 11 July 2012
Available online 20 July 2012

Keywords:
PEFC
GDL
Compression
Displacement factor
Contact resistance

ABSTRACT

This paper describes the use of an *in situ* analytical technique based on simultaneous displacement and resistance measurement of gas diffusion layers (GDLs) used in polymer electrolyte fuel cells (PEFCs), when exposed to varying compaction pressure. In terms of the losses within fuel cells, the ohmic loss makes up a significant portion. Of this loss, the contact resistance between the GDL and the bipolar plate (BPP) is an important constituent. By analysing the change in thickness and ohmic resistance of GDLs under compression, important mechanical and electrical properties are obtained. Derived parameters such as the 'displacement factor' are used to characterise a representative range of commercial GDLs. Increasing compaction pressure leads to a non-linear decrease in resistance for all GDLs. For Toray paper, compaction becomes more irreversible with pressure with no elastic region observed. Different GDLs have different intrinsic resistance; however, all GDLs of the same class share a common compaction profile (change in resistance with pressure). Cyclic compression of Toray GDL leads to progressive improvement in resistance and reduction in thickness that stabilises after ~10 cycles.

1. Introduction

The gas diffusion layer (GDL) plays a crucial role in the operation of polymer electrolyte fuel cells (PEFCs). The GDL enables gas to diffuse to and from the electrode surfaces, removes water from the electrode, provides electrical conduction between the current collector (bipolar plate) and the catalyst layer and provides a thermally conductive path to dissipate the heat produced at the catalyst. As such, the ideal properties for a GDL are for it to: be highly electrically and thermally conductive (note that some thermal resistance can be desirable for water management so that product water can move away from the electrode through the MPL as a vapour); have a large porosity to allow effective diffusion (yet maintain requisite mechanical properties); facilitate water removal from the electrodes by having the appropriate hydrophobic/hydrophilic properties. The two main varieties of GDL are the 'paper' and 'cloth' types, each made of carbon fibres and typically impregnated with polytetrafluoroethylene (PTFE). A wide range of GDL materials exist and their properties vary greatly [1].

A significant performance limitation for fuel cells is the ohmic losses associated with contact and bulk resistances. Of these ohmic losses, the contact resistance between the GDL and the land of the flow channels of the bipolar plate plays a significant part. Contact resistances are known to be greatly affected by the compaction force applied and the way the fuel cell is assembled. Studies have

* Corresponding author. Tel.: +44 20 7679 3310.
E-mail address: d.brett@ucl.ac.uk (D.J.L. Brett).
URL: http://www.ucl.ac.uk/centre-for-co2-technology

0378-7753/$ – see front matter © 2012 Elsevier B.V. All rights reserved.
http://dx.doi.org/10.1016/j.jpowsour.2012.07.021

shown the importance of cell compression on the overall performance of an operating fuel cell [2,3].

Despite the importance of compression regimes and the link between compression and electrochemical performance, relatively little studies have been reported in the literature and further research is required. Compression methods incorporating springs, integrated bladders and hydraulic or pneumatic presses have been described [4]. However, by far the most common method is the use of tie-rods of various numbers and positions, with controlled torque applied to the nuts at the end plates.

The pressure imposed to or exerted within a fuel cell can be measured in a number of ways. These include incorporating a pressure sensitive film into the cell (e.g Pressurex) [5], or using a load cell located between the nut and the cell endplate [6]. Pressure sensitive film requires the cell to be dismantled and therefore does not provide information about how the pressure changes with time. Load cells provide 'real time' data but do not take into account the losses within the system (frictional losses between mating surfaces), so the pressure exerted within the stack, experienced by the components, must be inferred.

Piezoresistive thin film sensor arrays have been demonstrated and allow 'real time' distributed pressure monitoring within operational fuel cells [7]; the technique provides valuable information for optimizing compression, results obtained show that the type and design of seals/gaskets is vital in this process. Other ways in which the ohmic losses can be affected include reactant gas pressure variations [8], flow-field geometry and dimensional changes in components such as the membrane material, which can change in thickness by a relatively large amount during hydration cycling [9].

The effect of compression force on fuel cell performance has been studied by Lee *et al.*, who showed that depending on the type of GDL material used, an optimum compression force exists [2]. However, this study used the bolt torque method of controlling force and as such is not particularly accurate or repeatable. Other *in situ* studies have used hydraulic presses [4] and screw arrangements [10] to try to improve the reproducibility of such testing. More fundamental studies such as those by Radhakrishnan *et al.* and Su *et al.* have examined the effects of compression on the GDL media *ex situ*, and have attempted to model the compressive effects [11,12]. Brett *et al.* employed a segmented current collector made using printed circuit board technology to capture the spatial variation of contact resistance across a cell and found that the way a fuel cell is put into compression using tie bolts has significant effect on the resistance distribution [13]. The findings of these studies show that as the compressive force increases there is a substantial decrease in contact resistance coupled with a decrease in the porosity of the GDL material. While the contact resistance reduction is desired, the decrease in porosity has the effect of limiting the pathways within the material and as such restricts the performance of the cell at high reactant utilizations.

Table 1 summarizes the range of materials and compression conditions previously reported in the literature. It can be seen that the nature of the GDL and the compaction range has a significant effect on the contact resistance measured. The bipolar plate (BPP) material is also known to affect the contact resistance [14].

In this paper, *in situ* analysis of various commercially available GDL materials is reported, showing how dimensional change and resistance response are affected when exposed to mechanical compression in the range relevant to practical PEFCs. In this study, a commercial instrument was used to control pressure exerted on a specially designed fuel cell, allowing the imposed force to be directly translated to the flow field plate using a floating piston system. By using 'real' flow-fields, the results better reflected the situation in practical fuel cells where issues such as 'tenting' (the intrusion of GDL into the open channel space) and localized compaction under land areas exist [19,20].

Table 1
Comparison of compression ranges and resistances reported in the literature for different BPP and GDL materials.

GDL material	BPP material	Compression range (MPa)	Resistance (mΩ cm^2)	Ref.
Toray H060	Plexiglas	0.48–2.41	N/A	[15]
Paper type	Graphite	0.25–3.5	45–23	[6]
SGL-10	–	0.15–3	6–2	[16]
Toray H Series	–	0.45–3.6	160–0.06[a]	[4]
ELAT	Stainless steel	0.42–0.92	28–14	[8]
ELAT	Graphite	3	10	[17]
ELAT	Graphite	0.4	13	[17]
Carbel CL	Poco graphite	0.5–3	30–10	[18]

[a] mΩ (not area specific).

2. Experimental methods

Experiments were carried out using a commercially available cell compression unit (CCU) (Pragma Industries SAS, France), which allows controlled compression of the GDL sample between two flow field plates while measuring the displacement change with a resolution of ±1 μm. The unit comes with a pre-set range for compression up to 2.5 MPa with a resolution of 0.01 MPa based on an active cell area of 6.2 cm^2, the bipolar plate flow field features a single serpentine design with land and channel thickness of 1.2 mm and 1.1 mm respectively. The unit operates under displacement or compression control, temperature control is possible to ±1 °C in the cell. When the unit is initiated the compression piston moves out to meet the 'floating piston' of the cell (Fig. 1) where an internal load cell and displacement sensor control the compression, depending on the operating control mode. The floating piston design allows the pressure that is exerted from the unit to be directly transferred onto the sample between the plates and has the added advantage of not being susceptible to the losses associated with the tie-rod method of construction. The CCU also ensures a much greater degree of reproducibility in the compression of samples due to the nature of its design.

Resistance measurements were achieved with an Iviumstat.XRi high current potentiostat (Alvatek Ltd, UK) using electrochemical impedance spectroscopy (EIS). EIS scans were run over a frequency range of 100 kHz to 0.1 Hz with an amplitude of +10 mV. The high frequency intercept with the real axis on the Nyquist plot was used as a measure of the bulk of the GDL and bipolar plate combined with the contact resistance between the two.

With the cell empty (i.e. no GDL sample) and hence with only a BPP–BPP interface, the resistance value measured with EIS was 36 mΩ cm^2 at 1.5 MPa. In the presence of the GDL materials between the BPPs the measured resistance is typically <20 mΩ cm^2, so attesting to the improvement in contact resistance achieved using a conformable material. The resistance values reported in this study are a summation of the BPP–GDL interface, fibre bulk resistance and GDL internal fibre connections and bulk system resistance.

The effective thermal expansion coefficient of the CCU was determined to be 1.92 μm °C^{-1}. Temperature control was achieved with an accuracy of <1 °C over the course of each experiment in a temperature controlled room. Dry nitrogen (calibrated mass flow controller: EL-FLOW, Bronkhorst, UK) was passed over one side of the cell at a flow rate of 50 ml min^{-1}, with the other side being sealed, so excluding water from the system. The flow-field of the CCU cell has a total land area of 3.3 cm^2 (i.e. 53% of active area of the cell).

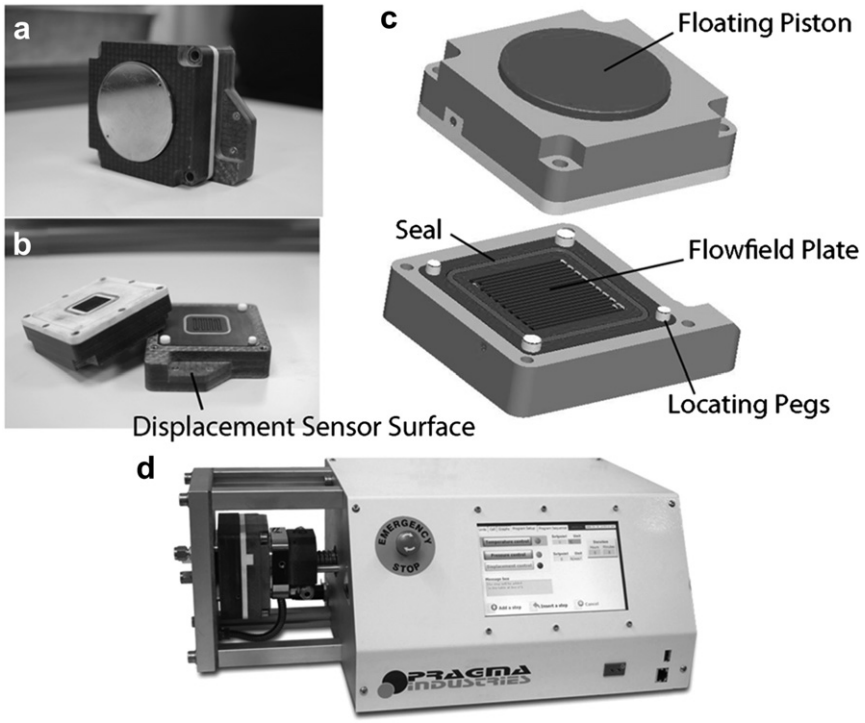

Fig. 1. Controlled compression unit cell. (a) The 'floating piston' is designed to exert pressure only upon the active area of the MEA, and (b) static flow-field that the piston presses against and provides the surface for the displacement sensor. (c) Floating piston cell design. (d) Cell compression unit (CCU); (images (c) and (d) courtesy of Pragma Industries SAS, France).

A range of commercially available GDL materials were tested (Table 2). The materials were all 'pure' GDL without microporous layers (MPL) and used as received.

Scanning electron microscopy (SEM) images were taken using a JEOL JSM6480LV (Jeol Ltd., Japan).

3. Results and discussion

3.1. Compression cycle

The compression cycle response of a sample of Toray H120 GDL can be seen in Fig. 2. The response indicates that after one cycle of compression to a maximum value of 2.5 MPa the GDL material exhibits irreversible compression resulting in a deficit between the initial displacement value and the value after the cycle that is 32% of the total displacement change. A similar lack of reversibility is shown in the resistance, resulting in a net reduction of 5.6 mΩ cm^2.

Fig. 3 shows an SEM image of the GDL sample, the compressed (land) and uncompressed (channel) are clearly distinguishable. Fig. 3(b) shows a close up of the land area where it can be observed that the carbon fibres are broken and compacted. This not only reduces the porosity of the material but also increases internal fibre connections, which may account for the lower resistance after the initial cycle. This can be compared to the open channel parts of where no compression has occurred.

Fig. 4 shows the effect of extreme compression up to many times operating compression of 12.5 MPa, this exaggerated compression illustrates the crushing problem. Part (a) shows the imprint made by the land, part (b) shows a close-up of the crushed zone with many short, well compacted fibres.

Table 2
Commercially available GDL samples tested.

Manufacturer	Type	Description
Ballard	1071HCB	Carbon cloth
	P75	Carbon paper
Sigracet	GDL 24 BA	Carbon paper with 5% PTFE loading
Toray	TGP-H-060	Carbon composite paper with 5% PTFE
	TGP-H-120	

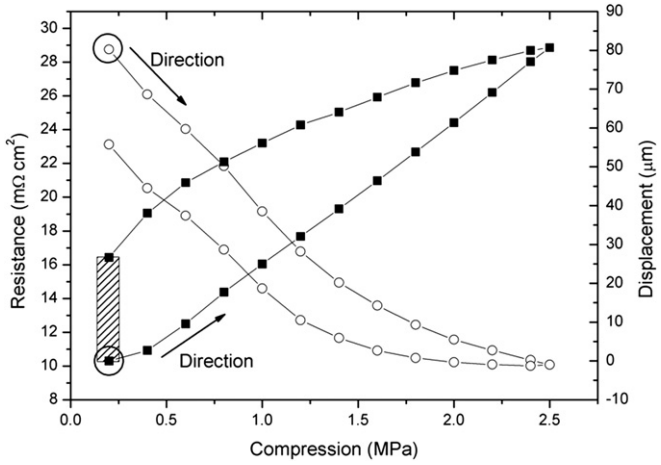

Fig. 2. The first compression cycle after initial loading of the GDL sample to 2.5 MPa and back to minimum compression of 0.2 MPa. Trends show the displacement (■) and resistance (○) relationship to compression for a sample of Toray H120, with the shaded area representing the extent of irreversible compression. The initial linear response for the displacement has a gradient of 37.5 μm MPa^{-1}.

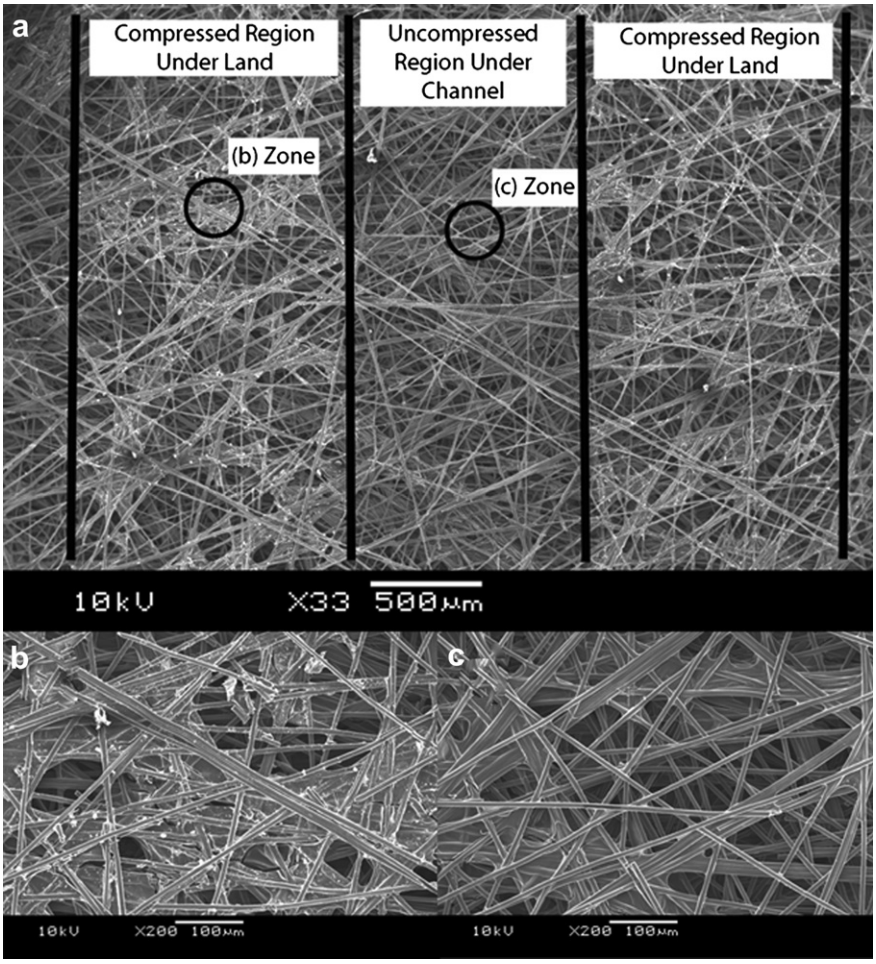

Fig. 3. SEM images of un-teflonated Toray paper showing: (a) the impression of the flow-field land made upon compression to 2.5 MPa with the black vertical lines as a visual aid, (b) a close up of the compressed zone under the land area showing broken fibres and (c) showing the uncompressed region from under the flow channel.

3.2. Compression reversibility

To examine reversibility of the compression effects, the CCU was programmed to return back to a minimum operating pressure of 0.2 MPa after each compression step. This enables the displacement and resistance response to be obtained before and after each compression step and thus determine the extent of irreversible compression. The compression reversibility characteristics are shown in Figs. 5–7.

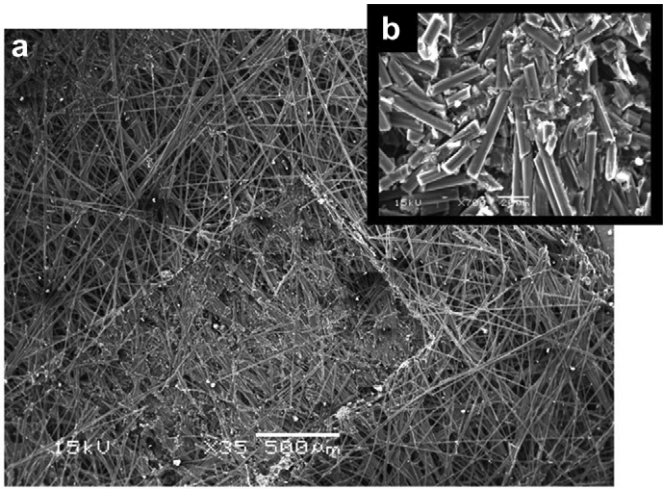

Fig. 4. SEM images of un-teflonated Toray paper showing: (a) the impression of the flow-field land made upon compression to 12.5 MPa, and (b) a close up of the compressed zone under the land area showing broken fibres.

It can be observed in Fig. 5 that the displacement of the sample increases in an approximately linear fashion in a similar way to that in Fig. 2. However, the gradient is lower at 31.8 μm MPa^{-1} compared to 37.5 μm MPa^{-1} for the monotonic increase in pressure without returning to minimum compression. This is considered to be due to the limited displacement reversibility of the GDL, which means that cycling between compressed and relaxed states leads to less net compression of the component. This may have useful practical consequences when formulating cell compression protocols.

The level of irreversible compaction is shown in the graph inset in Fig. 5. The first few cycles show that the GDL has only a slight (few microns) net compression effect. The degree of irreversibility increases with cycling and the extent of compression.

For the resistance (Fig. 6), a similar non-linear profile is observed to that of Fig. 2. The relaxed state (0.2 MPa, inset in Fig. 6) shows a net decrease in resistance with cycling. This may be due to improved contact between the GDL by virtue of the compacted broken fibres under the lands or tenting in the channels (intrusion of the fibres into the channels leading to new contacts between the GDL and the inner walls of the channels).

Fig. 7 shows the relationship between resistance and displacement as a piece of Toray H120 over a range of compression from 0.2 to 2.5 MPa. The insert shows the same relationship but all points

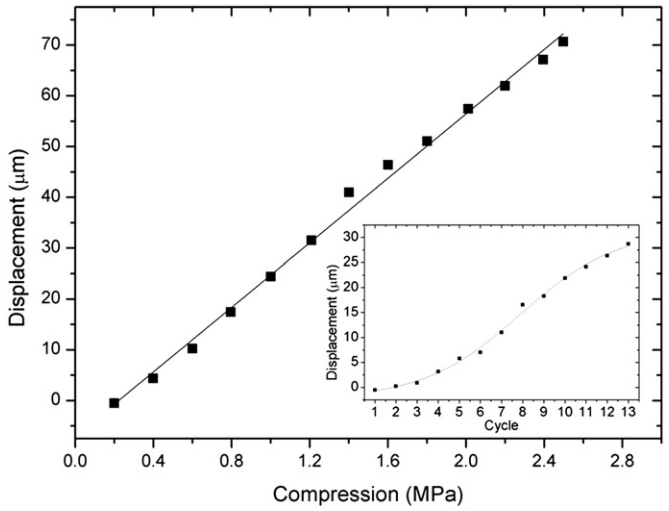

Fig. 5. Trend observed for Toray H120 displacement when compression is returned to 0.2 MPa between each step of increased compression on a single GDL sample. Insert: Irreversible displacement with increasing compression step as in the main figure (reduction of the thickness of the sample after each cycle, points are at 0.2 MPa).

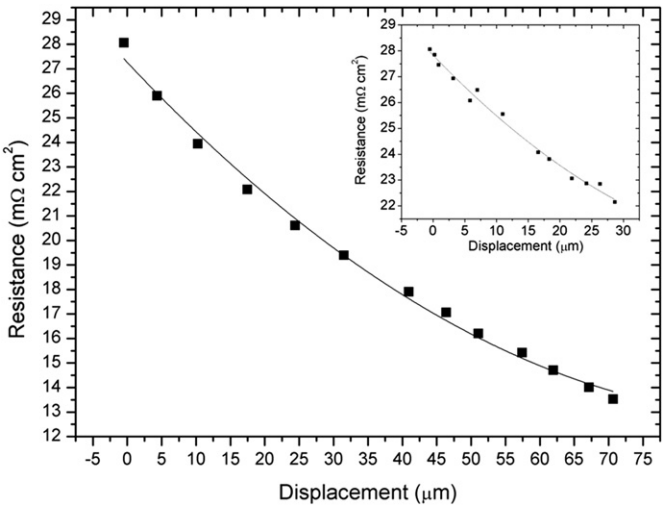

Fig. 7. Relationship between displacement and resistance response of Toray H120 from Figs. 5 and 6. Insert: Trend for values obtained at 0.2 MPa.

are at 0.2 MPa. Fig. 7 demonstrates that while the resistance decreases at a near constant rate in relation to displacement, the rate of decrease of resistance reduces as the displacement increases.

3.3. Comparison of various GDL materials

Fig. 8 shows the effect of compression force on the dimensional change and resistance of a range of commercially available GDL materials. During the initial phase of compression there is an engagement feature that can be seen in both the displacement and resistance traces for each of the GDL materials. The engagement feature does not appear to be dependent upon the type of the GDL due to difference in the trends observed by the two thicknesses of Toray material. This feature can be attributed to the initial interaction of the surfaces of the BPP and the fibres of the GDL.

Table 3 shows manufacturer data for GDL materials and results from this study. Note that the total resistance is composed mainly of the contact resistance, hence thickness has a small effect on the

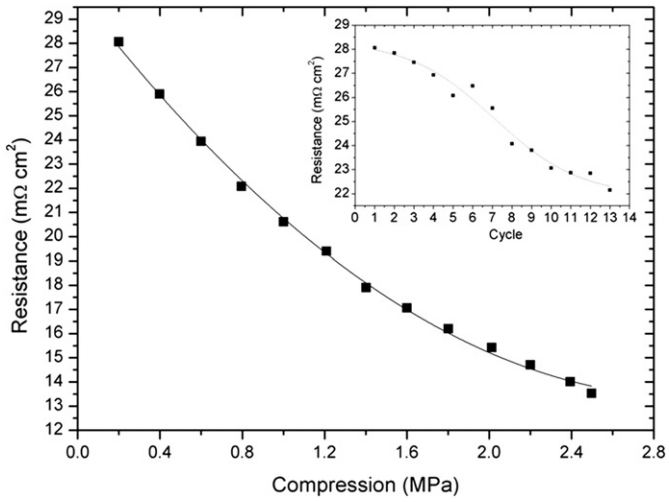

Fig. 6. Corresponding trend for Toray H120 the resistance response to the data in Fig. 5. Insert: Values for the resistance at 0.2 MPa after each cycle of compression.

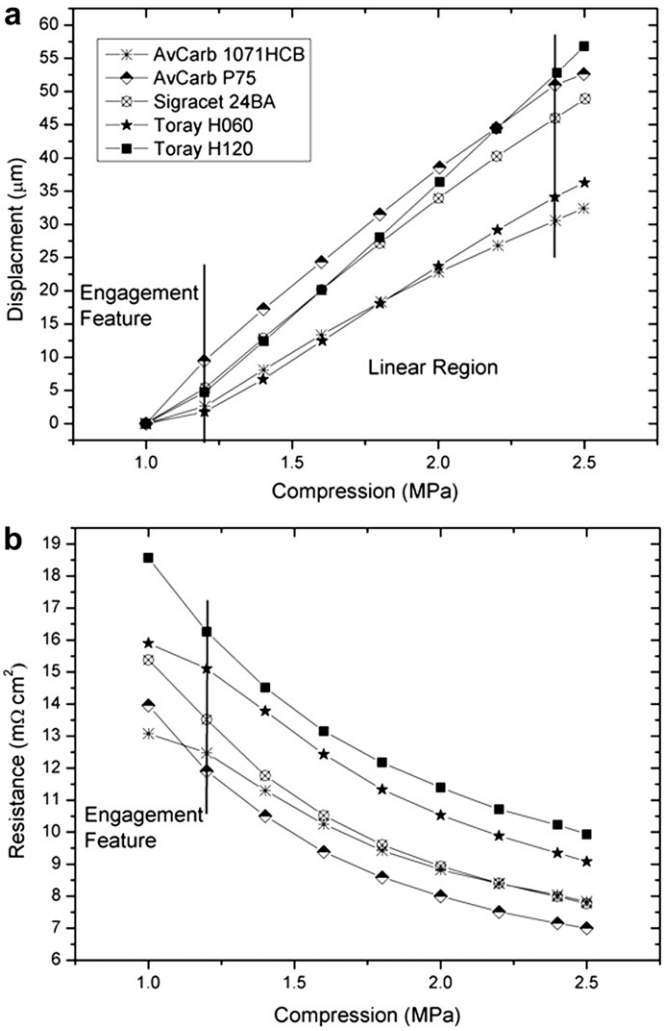

Fig. 8. (a) Displacement response comparison graph for various GDL materials tested *in situ* from 1 to 2.5 MPa compression; (b) corresponding resistance response.

Table 3
Comparison table of the rate of change of displacement with compression for various GDL materials from the linear region of Fig. 4.

GDL material	Material type	Thickness (μm)	Through-plane resistivity from manufacturer data (mΩ cm^2)	Measured resistance @ 1.5 MPa (mΩ cm^2)	Displacement factor (μm MPa^{-1})	Relative displacement factor (μm MPa^{-1} μm^{-1})
AVCarb 1071HCB	Cloth	220	7.7	7.70	22.4	0.102
AvCarb P75	Paper	200	7.4	7.11	33.8	0.169
Sigracet 24BA	Paper	200	<10.0	7.98	33.3	0.167
Toray H060	Paper	190	1.9[a]	9.42	27.6	0.145
Toray H120	Paper	370	3.0[a]	9.96	40.3	0.109

[a] mΩ (not area specific).

total resistance (cf. Toray H060 and H120). The 'displacement factor' describes the change in dimensional thickness with compression force, i.e. the gradient of the linear section for each GDL material from Fig. 8(a). This represents a convenient metric for comparing the mechanical properties of different GDL materials. Of the materials that are of comparable thickness (190–200 μm) and construction (paper type) the Toray H060 exhibits the lowest displacement factor; however, there is a range of values for materials in this category. The carbon cloth, AvCarb 1071HCB, has the lowest displacement factor and therefore most resistant to dimensional change with compression. The 'relative displacement factor' (MPa^{-1}) shows the displacement factor normalized for thickness; i.e., change in thickness with pressure divided by initial thickness (μm MPa^{-1} μm^{-1}). This factor shows that the Toray materials have significantly different responses even though the intrinsic material construction is the same.

From Fig. 8(a), the displacement trend includes a large linear region from 1.2 to 2.4 MPa. This linear region is important as it represents the range over which fuel cells commonly operate (Table 1) and as such shows how the GDL material reacts to changes in compression during operation. It is apparent from analysis of the linear fits of this region, Table 3, that the type of material is important in determining the response of the GDL to compressive force.

The linear trend for the displacement graph contrasts with a curved profile for the resistance response, shown in Fig. 8(b). Each of the materials starts from a different initial resistance and then decreases with increasing pressure, following very similar profiles for each of the paper-based GDLs. The carbon cloth exhibits a shallower response, the resistance decreasing at a slower rate with increasing pressure than the paper type GDLs. Note that although the paper type materials are generically similar, the fabrication methods vary and the structures can be quite different [1].

These results imply that there is an 'intrinsic' resistance associated with each GDL material manifest under minimum compressive force. The change in resistance is a function of the class of material (paper or cloth). The difference between the initial resistances of the two Toray papers (each made of the same material) is attributed to the difference in thickness.

3.4. Resistance and displacement relationship

The relationship between the displacement and resistance response gives additional insight into the way the GDL responds in

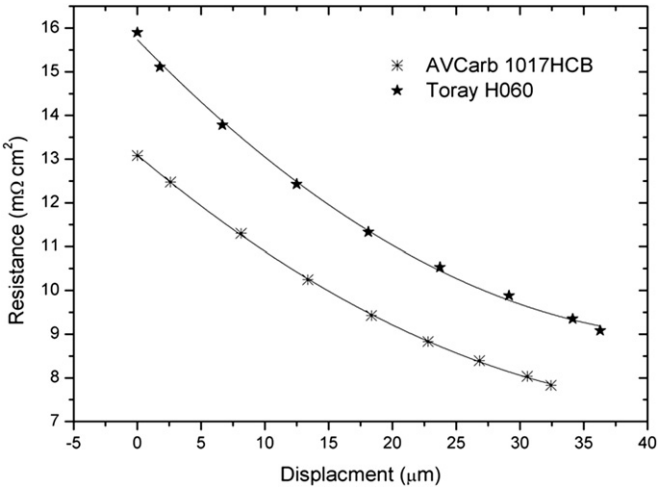

Fig. 9. Relationship between the resistance response and the displacement for Toray H120 and AVCarb 1071HCB GDL samples with a fit as a guide to the eye. This figure shows the response over the compression range between 0.2 and 2.5 MPa. The compression was not returned to the minimum in-between each point.

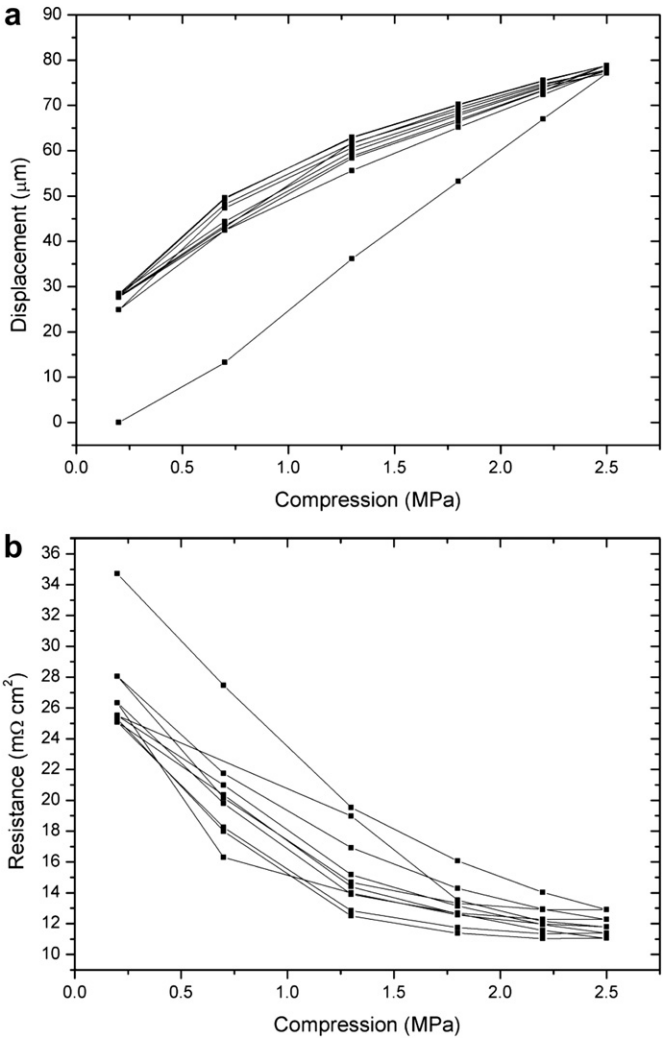

Fig. 10. (a) Depicts the multiple compression cycling effect on the thickness of a Toray H120 GDL with (b) showing the sample resistance response.

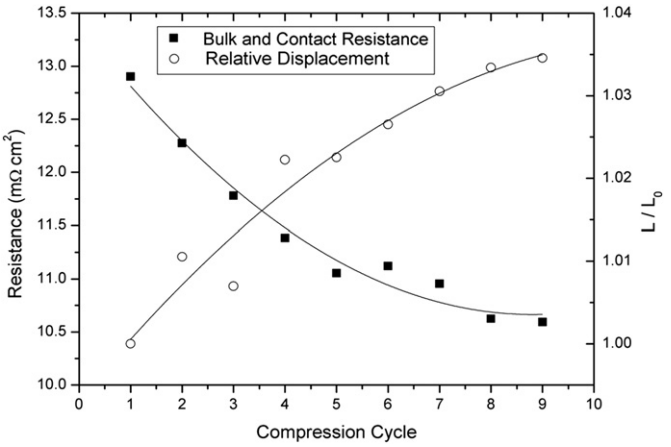

Fig. 11. Graph depicting the multiple cycling effects on Toray H120 after cycling of compression from 0.2 to 2.5 MPa. The measurements are each taken after stabilization at maximum compression for each cycle. The displacement trend shows that the material compresses 103.5% of the original maximum displacement and the resistance response tends towards a plateau at 9.8 Ω cm^2.

a fuel cell environment, as shown in Fig. 9. Initially, the resistance increases with a relatively small decrease in displacement; however, this is non-linear and a progressively greater displacement is associated with resistance drop. Fig. 9 compares Toray H120 and AVCarb 1071HCB with extremes of performance (see Fig. 8). However, with the exception of the initial resistance, each follows a very similar profile of dimensional and resistance change.

3.5. Cyclic behaviour

The durability of GDL materials is important as they have to operate for many thousands of hours in practical applications. During operation there are several factors that may cause dimensional change in a fuel cell. Thermal cycling, antagonised by components with different thermal expansion coefficients (i.e., BPP materials, metallic backing plates or end plates or the cell tie rods) and hydration cycling of the electrolyte and GDL, can all impose mechanical stresses and consequent strain in PEFC stacks.

Fig. 10 shows the multiple cycle profile for a GDL (Toray H120) sample. The displacement response from Fig. 10(a) shows an initial straight line trend followed by the secondary curved trend that is repeatable and does not vary significantly when compression is increasing or decreasing. The resistance trend in Fig. 10(b) shows that the difference between initial and secondary trend of the displacement response is not repeated for resistance, it also shows that the trend is repeatable after a number of compression cycles.

Fig. 11 shows the maximum and minimum of the displacement and the resistance response respectively for each cycle of compression. Each response shows a trend towards a plateau in the data at approximately nine cycles of compression from 0.2 to 2.5 MPa. This suggests that the relaxation of the GDL material due to the compression occurs after a relatively low number of cycles. The displacement figure rises 3.5% from the initial maximum, suggesting a small reduction in thickness and therefore porosity of the material. The resistance response at maximum compression corresponds to a ~20% reduction in ohmic resistance of the GDL material over the number of cycles measured.

4. Conclusions

This study demonstrates the use of a new commercially available instrument capable of controlling the compaction pressure while measuring the displacement (with 1 μm resolution) of PEFC MEAs or components. Here, the compaction properties of commercial GDL materials in contact with practical BPP flow plate designs are investigated at the same time as the effect on the internal resistance of the GDL and GDL/BPP contact resistance. Derived parameters such as the displacement factor facilitate selection of different GDL materials based on mechanical criteria. This work further demonstrates the importance of compression in fuel cell applications and shows the dominant properties of the contact resistance between the BPP and GDL.

The results show that hard won millivolts of performance, brought about by catalyst and membrane advances, can be lost through poor choice of GDL material or compression engineering (e.g. for operation at 1 A cm^{-2}, every mΩ dropped in the GDL equates to a mV of voltage loss). Increasing compaction pressure always leads to a decrease in resistance; however, this relationship is non-linear and there are diminishing returns on resistance decrease when increasing compacting force that can lead to deleterious effects such as GDL damage, loss of porosity and tenting.

For Toray paper, compaction becomes more irreversible with compression pressure – at low compression there is only slight net reduction in GDL thickness but there is no evidence that an 'elastic' region exists. It was found that different GDLs have an intrinsic resistance that is a function of their thickness and material/structural composition. Subsequent increase in compaction pressure leads to a very similar reduction in total resistance that is common to all of the paper type GDLs.

Acknowledgement

The authors would like to acknowledge EPSRC Supergen Fuel Cells for supporting the work of Mason and Brett (EP/G030995/1), the EPSRC 'Mind the Gap' UK/India project (EP/I037024/1) for supporting Millichamp, the Centre of Applied Energy Research ltd (CAER) for El-Kharouf's studentship, Advantage West Midlands (AWM) for Science City funding, and EPSRC (Contract No: EP/E034888/1). Innovative Uses for Advanced Materials in the Modern World (West Midlands Centre for Advanced Materials Project 1 and 2), with support from AWM and part funded by the European Regional Development Fund (ERDF).

References

[1] A. El-kharouf, T.J. Mason, D.J.L. Brett, Bruno G. Pollet, J. Powers Sources, in press.
[2] W.k. Lee, C.H. Ho, J.W. Van Zee, M. Murthy, J. Power Sources 84 (1999) 45–51.
[3] C. Wieser, A. Helmbold, E. Gulzow, J. Appl. Electrochem. 30 (2000) 803–807.
[4] L. Wang, L. Zhang, J. Jiang, Appl. Mech. Mater. 44–47 (2011) 2399–2403.
[5] J. Malzbender, R.W. Steinbrech, J. Power Sources 173 (2007) 60–67.
[6] W.R. Chang, J.J. Hwang, F.B. Weng, S.H. Chan, J. Power Sources 166 (2007) 149–154.
[7] R. Montanini, G. Squadrito, G. Giacoppo, J. Power Sources 196 (2011) 8484–8493.
[8] J. Ihonen, F. Jaouen, G. Lindbergh, G. Sundholm, Electrochim. Acta 46 (2001) 2899–2911.
[9] S. Slade, S.A. Campbell, T.R. Ralph, F.C. Walsh, J. Electrochem. Soc. 149 (2002) A1556–A1564.
[10] J. Ge, A. Higier, H. Liu, J. Power Sources 159 (2006) 922–927.
[11] V. Radhakrishnan, P. Haridoss, Int. J. Hydrogen Energy 35 (2010) 11107–11118.
[12] Z.Y. Su, C.T. Liu, H.P. Chang, C.H. Li, K.J. Huang, P.C. Sui, J. Power Sources 183 (2008) 182–192.
[13] D.J.L. Brett, A.R. Kucernak, P. Aguiar, S.C. Atkins, N.P. Brandon, R. Clague, L.F. Cohen, G. Hinds, C. Kalyvas, G.J. Offer, B. Ladewig, R. Maher, A. Marquis, P. Shearing, N. Vasileiadis, V. Vesovic, ChemPhysChem 11 (2010) 2714–2731.
[14] D.J.L. Brett, N.P. Brandon, J. Fuel Cell Sci. Technol. 4 (2007) 29–44.
[15] A. Bazylak, D. Sinton, Z.S. Liu, N. Djilali, J. Power Sources 163 (2007) 784–792.
[16] X.Q. Xing, K.W. Lum, H.J. Poh, Y.L. Wu, J. Power Sources 195 (2010) 62–68.

[17] R.C. Makkus, A.H.H. Janssen, F.A. de Bruijn, R.K.A.M. Mallant, J. Power Sources 86 (2000) 274–282.
[18] D.P. Davies, P.L. Adcock, M. Turpin, S.J. Rowen, J. Appl. Electrochem. 30 (2000) 101–105.
[19] I. Nitta, S. Karvonen, O. Himanen, M. Mikkola, Fuel Cells 8 (2008) 410–421.
[20] J. Kleemann, F. Finsterwalder, W. Tillmetz, J. Power Sources 190 (2009) 92–102.